Journal of Electroanalytical Chemistry 734 (2014) 53–60

Contents lists available at ScienceDirect

Journal of Electroanalytical Chemistry

journal homepage: www.elsevier.com/locate/jelechem

Hydrogen sorption and desorption related properties of Pd-alloys determined by cyclic voltammetry

A.V. Uluc [a], J.M.C. Mol [a], H. Terryn [b,c], A.J. Böttger [a,*]

[a] Delft University of Technology, Department of Materials Science and Engineering, Mekelweg 2, 2628 CD Delft, The Netherlands
[b] Vrije Universiteit Brussel, Research Group Electrochemical and Surface Engineering, Pleinlaan 2, B-1050 Brussels, Belgium
[c] Materials Innovation Institute (M2i), Mekelweg 2, 2628 CD Delft, The Netherlands

ARTICLE INFO

Article history:
Received 11 June 2014
Received in revised form 13 August 2014
Accepted 18 September 2014
Available online 30 September 2014

Keywords:
Hydrogen
Cyclic voltammetry
Pd-alloys
H absorption
H desorption

ABSTRACT

In this research we present a fast and quantitative electrochemical method – based on cyclic voltammetry (CV) – to screen the hydrogen (H) sorption (adsorption and/or absorption) and desorption behavior of Pd-based alloys. The method consists of a first step in which specimens are potentiostatically loaded with H, followed by a second step in which a CV experiment is performed with a wide-range potential sweep. During the second step, oxidation of H occurs as well as the formation of oxides and their consequent reduction. The H-loading and the CV start potential are the same so that H oxidation is not influenced by other surface reactions as it is the first process to take place. The method is applied to different Pd-alloys (Pd–Au, Pd–Mo–Cu) and it enabled to elucidate the differences in H-sorption/desorption properties of the alloys. X-ray diffraction (XRD) and scanning electron microscopy (SEM) are used to investigate changes in the structure as a function of the H-loading times. It was shown with this work that (i) the phases present in the microstructure have a significant effect on the amount of hydrogen absorbed and the kinetics of absorption, (ii) even very small amounts of desorbed hydrogen can be detected by CV and (iii) alloying elements affect hydrogen sorption/desorption behavior of Pd-based alloys and the interaction strength of H with the surface or the bulk.

1. Introduction

Palladium-based alloys are applied in membrane reactors to enhance the efficiency of industrially important chemical reactions [1–4] and in hydrogen production by steam reforming and water gas shift reaction [5–7]. Pd-alloys are also applied in thin film hydrogen sensors [8]. The lifetime and the performance, i.e. the permselectivity of membranes and the quality of sensors of Pd-based alloys is largely determined by hydrogen absorption and adsorption properties. The lifetime is mainly limited by hydrogen embrittlement when absorption of hydrogen causes hydride formation that is accompanied by large volume changes up to 10% (for pure Pd), causing microstructural changes and ultimately breakdown of the material [9]. The performance of Pd-based alloys, catalytic properties and sensing quality are influenced by surface poisoning [10–13] and in some cases by surface segregation [14,15]. Both adsorption and absorption properties are affected by the amount and type of the alloying elements. H-embrittlement can be reduced by alloying because absorption properties are changed such that the formation of hydrides (β-phase) is prevented under given process conditions, i.e. when the material stays in the α phase [9]. Alloying also changes adsorption properties which allows to reduce the susceptibility to surface poisoning [16] and to optimize the performance of sensors [17].

In this paper an electrochemical approach was utilized to study the hydrogen sorption and desorption reactions of bulk Pd–Au and Pd–Mo–Cu alloys with several tens of micrometer thickness by combining potentiostatic loading with voltammetry. Alloys chosen are promising candidates for membrane technology, particularly for hydrogen gas purification due to their resistance to surface poisoning and H embrittlement. Cyclic voltammetry (CV) is a useful technique in studying sorption/desorption mechanism of hydrogen and oxygen on various materials [18]. This is mainly because it reveals information on these mechanisms through well studied reactions, e.g. formation of adsorbed hydrogen (Volmer adsorption) or electrochemical desorption of hydrogen into the solution (Heyrovsky desorption) in one relatively fast scan. Another advantage of the method is the possibility of detecting very low amounts of H in the material. Czerwinski et al. [19–21] investigated the absorption/desorption properties of hydrogen in Pd using CV in

* Corresponding author.
E-mail addresses: A.V.Uluc@tudelft.nl (A.V. Uluc), A.J.Bottger@tudelft.nl (A.J. Böttger).

http://dx.doi.org/10.1016/j.jelechem.2014.09.021
1572-6657/

acidic and basic solutions. In these works the H-loading potential was related to the amount of H absorbed by the material; in their thin specimen the α and β phases form and show two distinct peaks in the anodic oxidation region. Lukaszewski et al. [22–25] investigated the hydrogen absorption behavior and the chemistry of the surface oxides of Pd–Au alloys. They identified the Pd-rich and Au-rich oxide forming species by investigating the oxide reduction peak observed in the CV.

Although there has been extensive research in the past on H in Pd-alloys, still the effect of alloying on H absorption is unknown for a wide range of electrochemical H-loading durations including low H content region (at room temperature: α-phase, $[H]/[M] \leqslant 0.05$), the two phase region (α + β-phase, $0.05 \leqslant [H]/[M] \leqslant 0.6$) and the H saturation region ($[H]/[M] \geqslant 0.6$). In this paper a wide range of loading times is used, which allowed to distinguish the H-sorption behavior of these alloys in the earlier stages when the system is not yet stable and later stages when the system reaches a steady state.

Different terms are generally used to describe the position or state of a hydrogen atom at the surface or in the bulk of material. In this paper the following nomenclature was used: (i) *Adsorption* refers to the accumulation of hydrogen (physisorbed or chemisorbed) at the surface and also includes the subsurface hydrogen, (ii) *Absorption* refers to the initially adsorbed hydrogen that has diffused into the bulk of the lattice, (iii) *Sorption* includes both adsorption and absorption phenomena and (iv) *Desorption* is the inverse of sorption; it defines the hydrogen that leaves the system through the surface (with an oxidation reaction) of the sample and diffuses into the solution.

2. Experimental procedure

The materials used for this study were 50 μm foils of pure Pd, Pd alloyed with Au ($Pd_{95}Au_5$, $Pd_{90}Au_{10}$, $Pd_{75}Au_{25}$) and Pd alloyed with Mo and Cu ($Pd_{85}Mo_{10}Cu_5$). The foils were obtained from Philips Research Laboratories in Eindhoven, The Netherlands. The samples were prepared from these foils by cutting pieces of 5 mm × 10 mm. Samples were attached to a steel wire by spot welding. The connection and the part of the wire that was inside the solution were painted with a lacquer resistant at highly basic solution. Prior to painting, both sides of the sample were washed first with acetone and then with ethanol, followed by drying with N_2, in order to dissolve any grease or similar contamination. The reference electrode was a saturated standard calomel electrode (SCE) and the electrolyte used was a 1 M KOH (Sigma Aldrich, purity ⩾85%, pH ∼ 13.1) solution. Finally, platinum was used as the counter electrode. Although in some cases [22–25] the solution is deaerated by bubbling Ar or N_2 gas prior to and/or during the experiment, our experiments were performed without bubbling gas since no effect of deaeration on results was found.

For the cyclic voltammetry experiments, a Potentiostat Autolab PGSTAT 12 was used. During the experiments, the potential was swept between −1.2 V and 0.5 V with a sweep rate of 0.01 V/s and starting at −1.2 V. The potentiostatic H-loading potential was selected as −1.2 V. Loading times were varied from 25 s to 8 h, so that the hydrogen adsorption/absorption behavior of the materials in α-, α + β- and β-phases is covered. The sequence of the electrochemical experiments is shown schematically in Fig. 1 and was as follows: (1) two repeated cycles of CV (Fig. 1a and b), (2) potentiostatic hydrogen loading at −1.2 V and (3) two repeated cycles of CV (Fig. 1c and d). The sample was not removed from the solution in between the steps mentioned above and the temperature was fixed at 300 K. All potentials are referred to SCE in this paper. Traditionally, the current density in CV experiments is expressed per unit area (A/cm^2). Since the amount of hydrogen absorbed depends also on the volume of the Pd samples, the data are expressed per unit volume (A/cm^3) to take into account the effect of small volume differences between the samples.

X-ray diffraction (XRD) was used to determine the phases present in the material upon different H-loading times. X-ray powder diffraction (XRPD) patterns were recorded in a Bragg–Brentano geometry in a Bruker D8 Advance diffractometer equipped with a Vantec position sensitive detector and graphite monochromator [26]. Data collection was carried out at room temperature using monochromatic Co Kα radiation (λ = 0.179026 nm) in the 2θ region between 40° and 140°, step size 0.04° 2θ and measuring time per step 2 s. The samples were placed on a Si {5 1 0} substrate and rotated during measurement. Scanning Electron Microscope (SEM) was utilized to investigate surface related changes (e.g. segregation) upon H-loading. The SEM was a JEOL JSM 6500F from Japan Electron Optics Ltd with a hot field emission gun and is equipped with a Thermo Fisher Ultradry EDS detector with Noran System 7 data-acquisition and data-analysis software. The backscattered electron detector (BSE) was an Autrata type.

3. Results and discussion

In this section the results of the electrochemical methods that were applied on Pd, Pd–Au and Pd–Mo–Cu will be presented and discussed. The range of alloying was chosen such that both the single phase ($Pd_{75}Au_{25}$ and $Pd_{85}Mo_{10}Cu_5$) and two-phase ($Pd_{95}Au_5$ and $Pd_{90}Au_{10}$) systems were investigated. A wide range of potentiostatic loading times were applied in order to gain knowledge on both adsorption and absorption related properties of Pd-alloys. In the following sections, before going into a detailed discussion on H adsorption/absorption properties of different alloys, a description of a typical CV scan will be given with the definitions of different regions, including the reactions taking place. Next, the method for quantification for both the CV scans and potentiostatic loading curves will be described. This will be followed by a discussion on H sorption/desorption properties of the Pd-alloys.

3.1. Description of a CV scan for Pd-alloys

A typical CV curve for $Pd_{95}Au_5$ is given in Fig. 2. Hydrogen evolution and/or adsorption takes place at Region 1 and Region 3, whereas H-desorption (oxidation) occurs in Region 2.

Region 1 in Fig. 2 shows that the current is negative and decreasing. In this region, the discharge of H_2O occurs (Volmer reaction) which results in hydrogen adsorption on the electrode surface according to Eq. (1). This reaction takes place around a potential of −1.068 V vs. SCE in a solution of pH 13.1 [27]. This is the main reason for selecting a potentiostatic H-loading potential of −1.2 V, i.e. to ensure that the Volmer reaction takes place on the surface of the working electrode.

$$H_2O + e^- \rightarrow H_{ads} + OH^- \quad (1)$$

The adsorbed hydrogen can either diffuse into the bulk through absorption (Eq. (2)),

$$H_{ads} \rightarrow H_{abs} \quad (2)$$

or it can recombine with another adsorbed H atom (Tafel reaction) and diffuse away from the surface as is given in Eq. (3):

$$H_{ads} + H_{ads} \rightarrow H_2 \quad (3)$$

Sweeping the potential from Region 1 towards Region 2, once the current is in the anodic region, the hydrogen that was adsorbed and/or absorbed in Region 1 starts to desorb, forming the hydrogen desorption peak. Sweeping the potential further until the switching potential (E_s = 0.5 V) leads to PdO formation (Region 4 in Fig. 2) and oxygen evolution (Region 5 in Fig. 2). During the reverse scan, oxy-

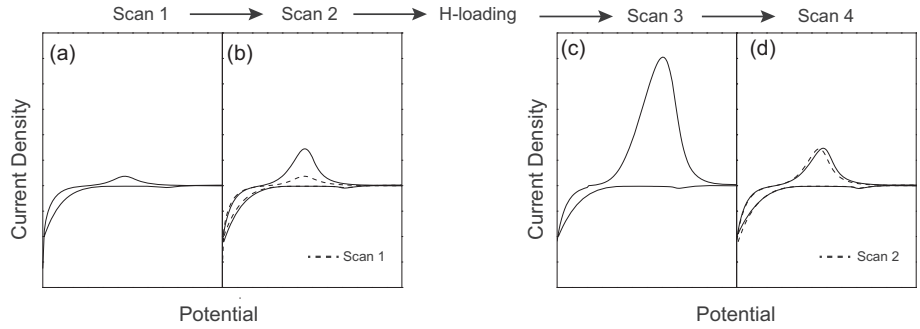

Fig. 1. Experimental scheme: CV scans before H-loading (a) scan 1, regarded as a cleaning/reference step; (b) scan 2; CV scans after H-loading (c) scan 3; (d) scan 4.

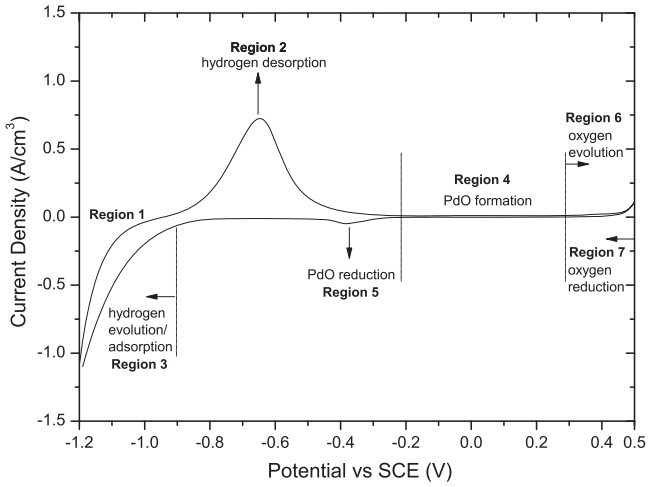

Fig. 2. A typical CV scan performed on $Pd_{95}Au_5$ in a 1 M KOH solution. Starting and switching potentials are −1.2 V and 0.5 V, respectively. Sweep rate is 0.01 V/s. Different reaction regions of hydrogen evolution/adsorption (Region 1 and Region 3), hydrogen desorption (Region 2), PdO oxidation and reduction (Region 4 and 5, respectively) and oxygen evolution (Region 6) are shown.

gen and PdO reduction takes place on the electrode surface (Region 7 and Region 5 in Fig. 2, respectively). This is followed by Region 3, where similar to Region 1, hydrogen is produced which can adsorb on the surface. Regarding the regions related to hydrogen sorption/desorption, Region 1 and Region 3 can be used to calculate the total amount of hydrogen evolved (H_2 gas and the hydrogen that is adsorbed) at the electrode surface and Region 2 is used to determine the amount that desorb out of the system.

3.2. Quantification of adsorbed and absorbed hydrogen for Pd-alloys

To quantify the amount of hydrogen that is sorbed and to establish if all the hydrogen that is evolved on the surface does sorb/desorb, the total charge Q (in C) involved in the reactions of Region 1, Region 2 and Region 3 are compared. Q is calculated by integrating the $I(t)$ after converting the potential axis of Fig. 2 to time axis as in Eq. (4):

$$t = \frac{|E(t) - E_i|}{\upsilon} \tag{4}$$

where $E(t)$ is the potential at time t (V), E_i is the initial/starting potential (V), υ is the sweep rate (V/s) and t is time (s). The E_i term in Eq. (4) is replaced by the switching potential E_s for the reverse scan.

The total charge Q calculated by integration of $I(t)$ is then used to calculate the amount of hydrogen. This implicitly assumes that each electron reacts with 1 H atom according to Eq. (1). If all the hydrogen atoms evolved are sorbed and also completely desorbed, then the following equations regarding scan 1 and scan 2 (see Fig. 1a and b) should hold:

$$\left(Q \text{ of Region } 1^{\text{scan } 1}\right) = \left(Q \text{ of Region } 2^{\text{scan } 1}\right) \tag{5}$$

$$\left(Q \text{ of Region } 3^{\text{scan } 1}\right) + \left(Q \text{ of Region } 1^{\text{scan } 2}\right) = \left(Q \text{ of Region } 2^{\text{scan } 2}\right) \tag{6}$$

After potentiostatic H-loading takes place, it should hold that:

$$(Q \text{ of hydrogen loading curve}) + \left(Q \text{ of Region } 1^{\text{scan } 3}\right) = \left(Q \text{ of Region } 2^{\text{scan } 3}\right) \tag{7}$$

The left side of these equations shows the total charges related to hydrogen evolution (adsorbed and/or evolved) and those on the right side are due to H-desorption. The comparison of the left and right side of Eqs. (5) and (6) averaged for 20 measurements shows that for scan 1, the difference between the total Q related to H evolution and H desorption is about 34%, whereas this difference for scan 2 is only 6%. The higher difference between the anodic and cathodic regions of scan 1 is attributed to the presence of contamination or oxide layers on the surface that reduce the sorption of hydrogen. It is also observed that the peak potential E_p of the hydrogen desorption peak (Region 2 in Fig. 2) of scan 1 and scan 2 are the same (−0.65 V vs. SCE). However, the total Q differs for these two scans (i.e., larger Q for scan 2), pointing to a larger amount of H adsorbed [18].

Similar to calculating the amount of H desorbing from the sample using the CV curves, integration of $I(t)$ vs. time plot of the potentiostatic loading curve was used to calculate the amount of hydrogen evolved during H-loading. The loading curves for the Pd–Au alloys are shown in Fig. 3. The loading curves of $Pd_{75}Au_{25}$ presented in Fig. 3c show different characteristics than that of $Pd_{95}Au_5$ and $Pd_{90}Au_{10}$ (Fig. 3a and b, respectively). The $Pd_{95}Au_5$ and $Pd_{90}Au_{10}$ samples show a region with slightly higher current densities (see arrows), whereas the $Pd_{75}Au_{25}$ sample does not show such region. The changes in the current (and hence the absorption property) are related to the phases present in the material as will be shown next. Different stages of the loading curves can be related to different phases as the α_{max} and β_{min} concentrations correspond to the charges in relation with inflexion points on the loading curves as shown by Lukaszewski et al. (Pd–Au and Pd–Pt) [28] and Hubkowska et al. (Pd–Ru) [29]. In the current work, direct phase identification was performed by means of X-ray diffraction at selected points (times of loading) of the loading curve. Fig. 4 shows the diffraction patterns of $Pd_{95}Au_5$ samples for different H-loading times. In Fig. 4a, the diffraction pattern of a fresh sample (before performing CV) is shown where the material is in the α-phase. The material is in the face-centered-cubic (FCC) structure

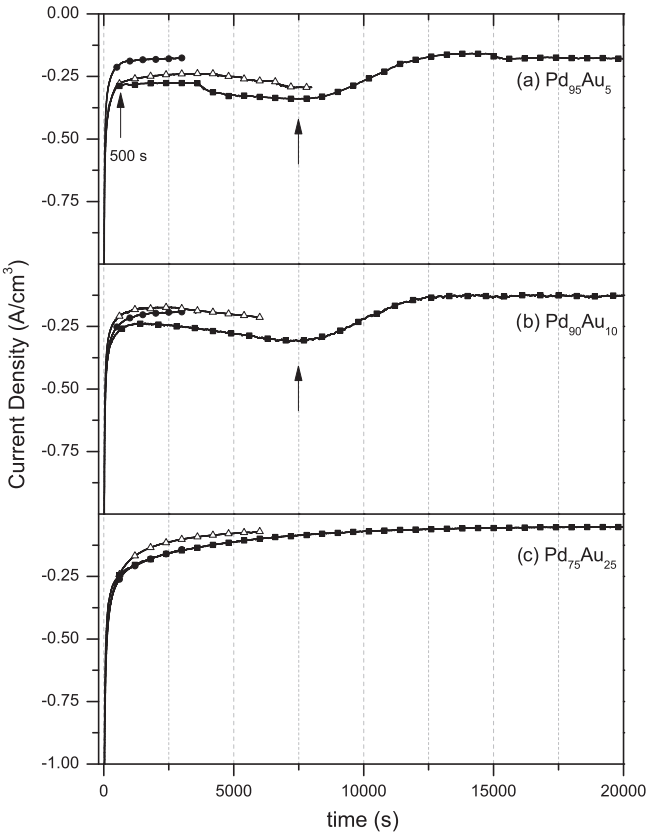

Fig. 3. Potentiostatic H-loading curves at −1.2 V for (a) $Pd_{95}Au_5$, (b) $Pd_{90}Au_{10}$, (c) $Pd_{75}Au_{25}$. The loading current goes through an increasing region followed by a decreasing trend in $Pd_{95}Au_5$ and $Pd_{90}Au_{10}$ samples associated with the $\alpha \rightarrow \beta$ transition. The $Pd_{75}Au_{25}$ alloy, however, does not show this behavior (stays in the one phase region throughout loading).

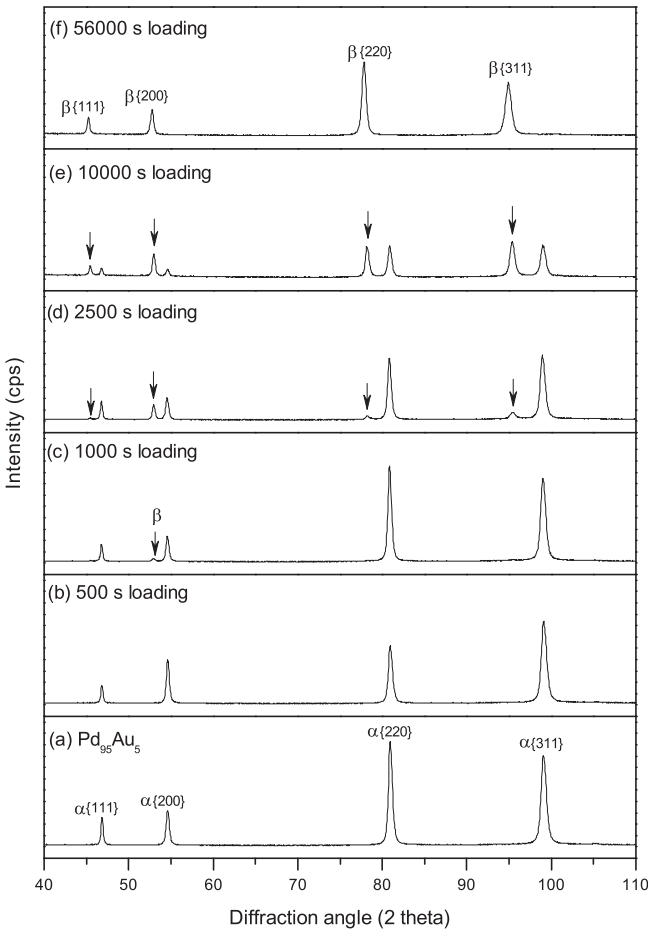

Fig. 4. XRD patterns of $Pd_{95}Au_5$ samples after different H loading times. (a) $Pd_{95}Au_5$ alloy showing FCC α-phase peaks. (b) After 500 s loading, the material is still in the α-phase, [H]/[Pd] cannot be calculated by XRD since a remarkable shift in peaks is not observed). (c) For the 1000 s loaded sample, the formation of β-phase (see arrow) [H]/[Pd] ~ 0.46. (d) After 2500 s loading [H]/[Pd] ~ 0.46 and (e) 10,000 s loading [H]/[Pd] ~ 0.46, the β-phase amount is increasing indicated by bigger β-phase peaks, (f) for a sample that was 56,000 s loaded [H]/[Pd] ~ 0.52, only the β-phase peaks are visible, indicating that the $\alpha \rightarrow \beta$ transformation is complete.

and H is expected to fill the interstitial sites upon loading. The XRD pattern for 500 s H-loading (Fig. 4b), is very similar to the diffraction pattern before loading, no additional diffraction peaks are observed. The 500 s loading corresponds to the initial part of the potentiostatic loading curve, where the current is abruptly decreasing, as indicated with an arrow in Fig. 3a.

In this region, the material is still in the α-phase and calculation of the hydrogen amount by means of XRD is difficult since a remarkable shift in diffraction peaks is not observed. The $\alpha \rightarrow \beta$ transition has started to take place for loading times around 1000 s. Diffraction patterns obtained at this stage of loading show the appearance of the β-{200} reflection next to the α-{200} reflection indicated by an arrow in Fig. 4c. The results of XRD when H-loading was performed for 2500 s and 10,000 s, which both corresponds to the higher current region of the loading curve (see arrows in Fig. 3a and b), are shown in Fig. 4c and d. It is clearly seen that the α and β phases coexist for these loading times and that the amount of β-phase increases in time, as indicated by a higher peak area of the β-phase for 10,000 s loading than 2500 s loading. For longer loading times (Fig. 4f) all the α-phase has transformed into the β-phase. The $Pd_{75}Au_{25}$ alloy does not show similar behavior of a change in the current density (see Fig. 3c) which suggests that this material stays in the one phase (α-phase) region throughout the loading. The corresponding H contents by means of CV will be discussed in the next sections.

3.3. Adsorption vs. absorption in the α-phase

The hydrogen desorption peak of the second scan is due to the total hydrogen sorbed during Region 3 in the first scan and Region 1 in the second scan (see Fig. 2). Since the amount of total hydrogen generated in these regions is very small, the second scans of Pd-alloys can be used to differentiate the adsorption properties of the materials. To determine if absorption readily occurs during the second scan, the number of hydrogen sites available on the sample surface and the amount of H evolved during the second scan was compared. Assuming a {1 1 1} orientation on the Pd surface and 1 H/Pd adsorption ratio on the surface [30], there are 3.79×10^{14} Pd sites available for H adsorption. The amount of hydrogen produced at the surface was calculated to be 1.41×10^{17} atoms (see Eq. (6) and Section 3.2 for information about the quantification method). This indicates that, even in Region 1 of the second scan when there is no H-loading performed on purpose, all the sites available for H near the surface are full. This means that, even in the very low H-loading amounts, absorption has started.

Fig. 5a shows a correlation between the mean peak potential of the hydrogen desorption peak and the percentage of Au in the Pd–Au alloy.

When the amount of Au in the alloys is small (Pd and $Pd_{95}Au_5$), the mean peak potential is significantly more cathodic compared to that of Pd-alloys of higher Au content. The more anodic peak potential of $Pd_{90}Au_{10}$ and $Pd_{75}Au_{25}$ samples could point to mainly

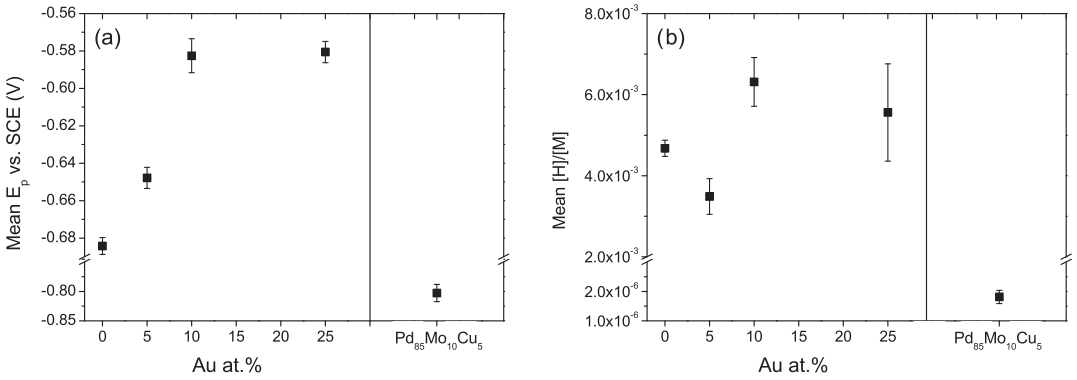

Fig. 5. (a) The mean peak potentials, (b) the mean [H]/[M] of minimum 20 measurements for Pd–Au and Pd–Cu–Mo systems. The second scans were used to determine the values.

three possibilities: (i) higher Au% samples sorb higher amounts of hydrogen and thus a longer time period is required to strip it all out; (ii) H diffusivity gets smaller with increasing Au% [31] so a longer time period is required for H to diffuse to the surface; or (iii) hydrogen is more strongly bound to the surface/bulk so that it is energetically more difficult to remove from the material. If the first option is correct, then the mean hydrogen content [H]/[M] should have the same trend as the mean peak potential with amount of Au in the Pd–Au alloy. However, it is shown in Fig. 5b that there is no clear correlation between the H content and the amount of Au in the alloy. In fact, for short loading times, the [H]/[M] is highest for $Pd_{90}Au_{10}$, somewhat lower for $Pd_{75}Au_{25}$ followed by pure Pd and smallest for $Pd_{95}Au_5$. Thus, the first option can be eliminated. The second and third options both remain as possible explanations. They are both feasible explanations. According to the third option, the peak shift is related to the interaction strength between the hydrogen and the surface or bulk sites of the alloy. As seen in Fig. 5a, this would suggest that the hydrogen is attached more strongly as the amount of Au in the alloys is increased. This is in good agreement with density functional calculations of Sonwane et al. [32,33], where the binding energies of hydrogen to the octahedral sites are calculated to be higher for Pd–Au alloys and lower for Pd–Cu alloys, with respect to pure Pd. For Pd–Cu–Mo system, the mean peak potential is the most cathodic one, and the hydrogen amount that is sorbed in the system is significantly lower than the Pd–Au alloys.

3.4. Hydrogen in the α+β and β phase regions

The CV scans of Pd alloys after H-loading up to 1000 s at −1.2 V are shown in Fig. 6. The direct observation for all materials is the shift of E_p to more anodic potentials as the loading time increases. This is because the potential axis of a CV curve can also be considered as a time axis. As the time of loading increases, there is more time needed to strip the H out of the samples. Also, the β-phase (once formed) needs to decompose into the α-phase during unloading which additionally could contribute to the time delay. It is also seen that different Pd–Au alloys with different percentages of Au have distinctly different shapes. While CV scans of $Pd_{95}Au_5$ look rather symmetrical in peak shape, the $Pd_{90}Au_{10}$ alloy shows a tail at the beginning of the hydrogen desorption peak whereas the $Pd_{75}Au_{25}$ shows a tail at the end. In Fig. 6d, the CV scans for Pd–Cu–Mo system is also shown for the same loading times. The shape in this case also consists of a hydrogen desorption peak with a tail at the end. Additionally, a high oxidation current is observed on the cathodic region right after the hydrogen desorption peak. This oxidation reaction prevents the hydrogen desorption peak current to drop to low values which makes the calculation of the hydrogen amount more difficult. In this case, by subtracting the charges (Q) involved in the reduction of PdO in the reverse scan from the total Q of hydrogen desorption of the forward scan, the hydrogen amounts were estimated.

As stated previously, the amount of hydrogen produced during potentiostatic loading can be compared with the hydrogen desorbing from the specimen during CV. The results for $Pd_{95}Au_5$ and $Pd_{75}Au_{25}$ for loading times up to 60,000 s are given in Fig. 7. As the loading time increases, the total hydrogen evolved also increases as expected. For the $Pd_{95}Au_5$ (Fig. 7a) the amount of H desorbed however first increases but then remains constant after loading times of about 10,000 s. Initially almost all the H produced also desorbs (91%), implying that almost all the H has been absorbed.

After longer loading times (>10,000 s) the material is saturated with H (about 0.5 [H]/[M]), the amount of desorbed H does not increase anymore, indicating that the material has absorbed the maximum amount of hydrogen for the given conditions. Similarly for the $Pd_{75}Au_{25}$ samples initially (loading time <10,000 s) there is an increase in the area of the desorption peak. After 10,000 s of loading, which corresponds to about 0.3 [H]/[M], there is a drop in the amount of desorbed H (down to about 0.25 [H]/[M]) and from then on that amount stays constant for all longer loading times. This reduction of desorbed H for $Pd_{75}Au_{25}$ after longer loading times is so far not understood. Both surface segregation and changes in the amount of defects in the material were investigated. Surface segregation (of Au) could hinder the dissociation of H_2 and therefore reduce the absorption of H atoms. Changes in the defect amount and type could lead to a reduction of the amount of desorbed H since defects could be traps for H. No surface segregation of Au [14,34] was observed by means of SEM. BSE data were used to first visually determine the Au-rich regions (higher brightness due to its higher weight than the Pd atoms) and then EDS was used to quantify the Pd:Au ratio. Analysis of the surface of $Pd_{75}Au_{25}$ with this method showed that a few Au-rich regions were present on the surface for both as-received material as well as the samples that were loaded longer than 20,000 s. But no clear increase of the amount of Au-rich regions was found. Changes in the amount or type of defects were also monitored by looking at XRD profiles and their line widths that in principle reflect local changes in the crystal structure [35], but no changes were found. Although experimentally not observed, our calculations based on work of Tomanek et al. [36] showed that segregation of Au to the surface of $Pd_{75}Au_{25}$ sample is expected to be more pronounced than for lower Au content samples. To summarize, even though proof of Au segregation was not found on the surface of $Pd_{75}Au_{25}$ samples, the possibility cannot be ruled out as an explanation of the observed difference between the hydrogen evolved during loading and the hydrogen desorbed from $Pd_{75}Au_{25}$ alloys.

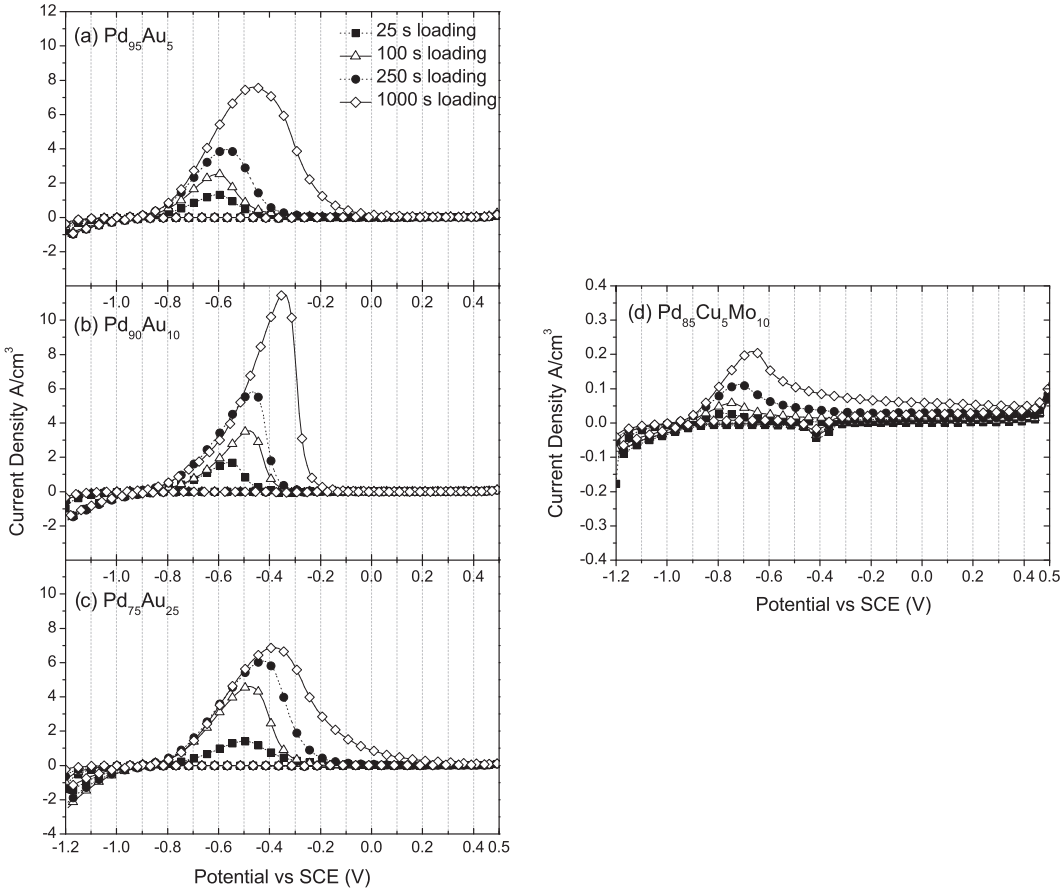

Fig. 6. CV scans of Pd–Au and Pd–Cu–Mo alloys after potentiostatic loading at −1.2 V for loading times between 25 s and 1000 s. (a) $Pd_{95}Au_5$, (b) $Pd_{90}Au_{10}$, (c) $Pd_{75}Au_{25}$, (d) $Pd_{85}Mo_{10}Cu_5$.

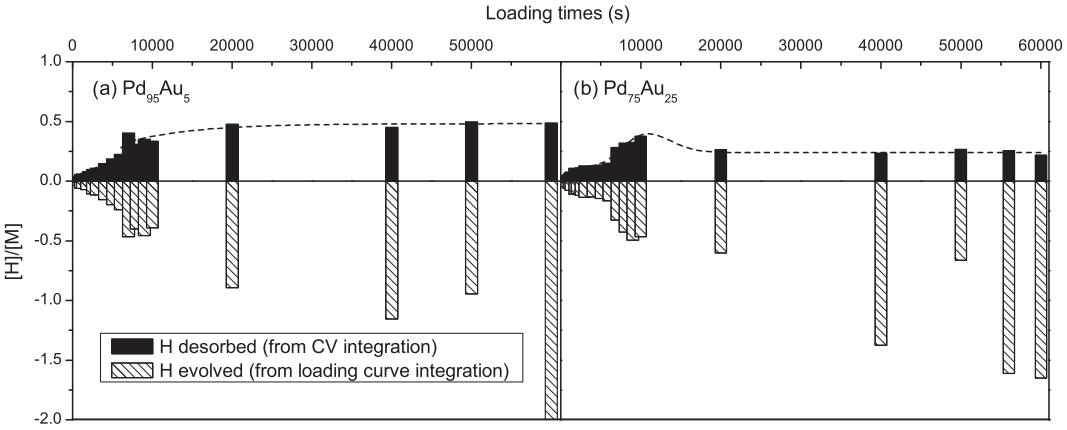

Fig. 7. Amount of hydrogen evolved during loading and amount of hydrogen desorbed during CV expressed as [H]/[M] for different loading times of (a) $Pd_{95}Au_5$, and (b) $Pd_{75}Au_{25}$.

Next, the relation between the amount of H desorbed as a function of loading time will be discussed. In Fig. 8a–c, the amount of desorbed H after various loading times for the Pd–Au alloys is presented. In Fig. 8a the results for the low H-loading times (up to 3000 s) are collected. Clearly, the $Pd_{75}Au_{25}$ sample absorbs the highest amount of hydrogen for the low loading times, however Fig. 8b shows that for higher loading times the $Pd_{75}Au_{25}$ samples desorbs less hydrogen than Pd_5Au_{95} and $Pd_{10}Au_{90}$. During the initial stages of H absorption where the system is away from a steady state, the H-absorption of different alloys is determined by reduction kinetics. This is reflected in the amounts of hydrogen evolved as shown in Fig. 7. For H-loadings up to 3000 s, the amount of hydrogen evolved is higher for $Pd_{75}Au_{25}$ than for $Pd_{95}Au_5$. This suggests that the H^+ reduction at the surface of the $Pd_{75}Au_{25}$ alloy is faster than the $Pd_{95}Au_5$ alloy. The amount of H eventually absorbed by the system is determined by thermodynamics. It is well known that the number of interstitial sites available for hydrogen decreases as the Au content in Pd increases [37,38], because the sites close to Au atoms are energetically less favorable for H. In particular, in Nanu et al. [38] the analysis of atom configurations by

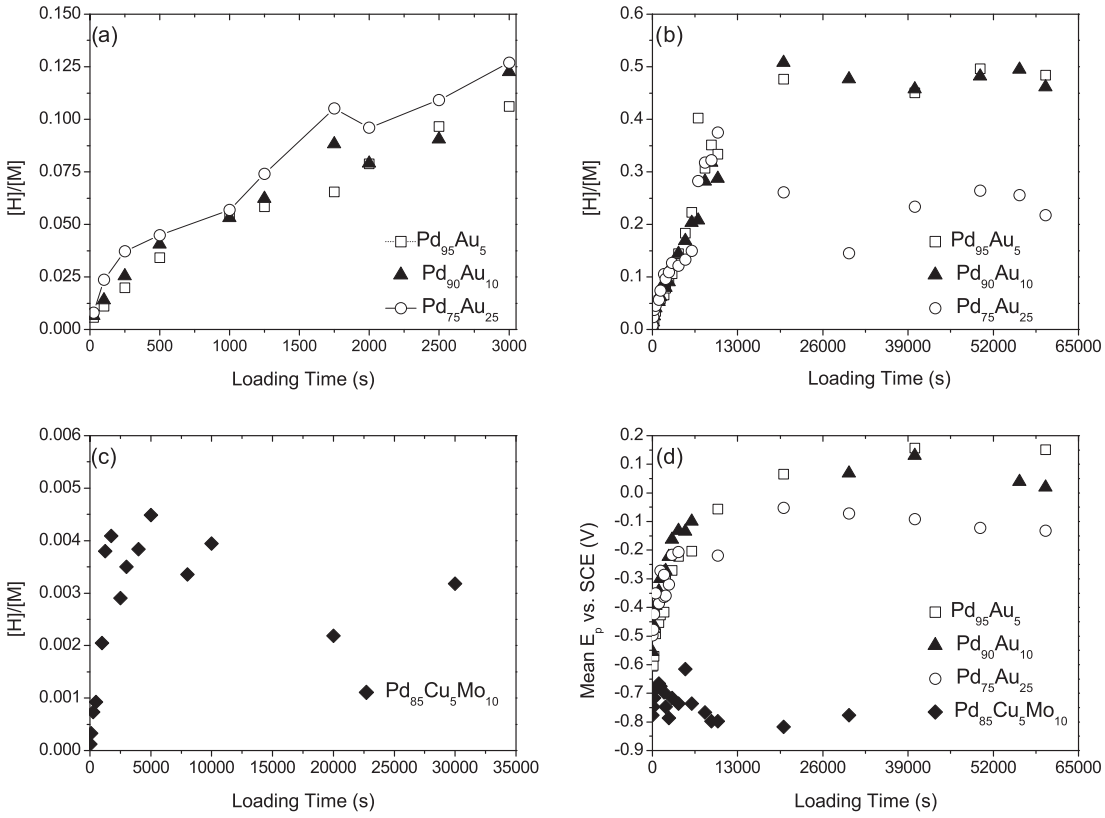

Fig. 8. Hydrogen content ([H]/[M]) and peak potential (E_p) vs. loading time for $Pd_{95}Au_5$, $Pd_{90}Au_{10}$, $Pd_{75}Au_{25}$ and $Pd_{85}Mo_{10}Cu_5$. (a) [H]/[M] for Pd–Au alloys with loading times at and below 3000 s, (b) [H]/[M] for Pd–Au alloys showing all loading times, (c) [H]/[M] for $Pd_{85}Mo_{10}Cu_5$ alloy showing all loading times, (d) E_p vs. loading time for Pd–Au alloys.

means of neutron diffraction showed that when the amount of Au in the Pd-based alloy is increased, also tetrahedral sites in the vicinity of Au atoms are occupied, whereas in pure Pd only octahedral interstitial site are occupied by H.

Moreover the local configuration of Au atoms around an octahedral site matters. This is consistent with the neutron diffraction experiments [37] and Mössbauer spectroscopy results [39] that indicated that the H atoms are repelled by Au atoms and consequently the interstitial sites in the vicinity of Au atoms are not preferably occupied by H atoms. The $Pd_{95}Au_5$ material absorbs less hydrogen than $Pd_{90}Au_{10}$ for loadings up to 3000 s (because of kinetics) but eventually higher amounts of hydrogen are absorbed, as is in accordance with the phase diagram [40]. In Fig. 8d, the mean peak potential (E_p) as a function of loading time is presented for Pd–Au alloys. In contrast with Fig. 5a (for low loading times), here the E_p is shifted to more cathodic potentials with increasing Au content. Lukaszewski et al. in their work [23] observed similar behavior and attributed the easier H-oxidation of Au-richer alloys to be kinetically originated by a probable change on the surface or the bulk characteristics of the samples upon Au% increase. Our results presented in Fig. 8b indicate that the amount of [H]/[Pd] is lowest for $Pd_{75}Au_{25}$ for the high loading times; the shift of the E_p of higher Au content samples is attributed to the fact that lower H amounts results in shorter times for the total H to desorb from the material. The observations regarding the E_p shift for low and high H amounts is also in accordance with recent work of Lukaszewski et al. [41]. Revisiting the discussion of the diffusivity of H in Pd–Au alloys that was considered before for very low H content (see Section 3.3), diffusion of H is not the determining factor in the observed peak potential shift (Fig. 8d) for the high H content. As Au% increases, the diffusivity of H decreases [31], so a peak shift to more anodic potentials is expected whereas the observed peak shift on Fig. 8d is towards more cathodic potentials. Thus, when only small amounts of hydrogen are absorbed, E_p reflects the H-metal binding strength or the diffusivity of H and for higher H contents the time needed to remove all the H is determining E_p.

4. Conclusions

In this research we used a fast and quantitative electrochemical method to screen the hydrogen sorption (adsorption and/or absorption) and desorption behavior. We showed that the method can be used to (i) determine the effect of phases present on the amount of hydrogen absorbed and the kinetics of absorption, (ii) quantify the amount of hydrogen desorbing (even for very small amounts) and (iii) identify the effect of alloying elements on hydrogen sorption/desorption behavior and the binding strength of H to the surface or in the bulk.

The method was applied to Pd-based alloys. Analysis of the H-loading current for different alloys (Pd, Pd–Au and Pd–Mo–Cu) shows that the phases present, i.e. α, α + β or β, influences the kinetics of H evolution and H uptake in the material. In particular, the hydrogen reduction kinetics is enhanced in the two-phase region. The amount of desorbing H, determined by the consecutive cyclic voltammetry scans, allowed to quantify the amounts of hydrogen even in the α-phase when about 0.05 H atoms per metal atom are present. Significant differences in H-sorption/desorption behavior are observed depending on the kind and amount of alloying elements present. Au and Cu–Mo addition can reduce the total amount of H that can be absorbed (long loading times). The parameter determining the total hydrogen uptake for low H-contents is the kinetics of H^+ reduction, whereas for long loading times the total amount of H in the material is determined by thermodynamics. The peak potential (E_p) of the CV scans may be an indication of

how strong the hydrogen is interacting with the surface or the bulk for low loading times and of the amount of H in the bulk for high loading times.

Conflict of interest

There is no conflict of interest.

Acknowledgements

The authors gratefully acknowledge R.W.A. Hendrikx and N.M. van der Pers for helping with XRD related sample preparations and discussions. We would also like to thank Irini Zacharaki for her experimental support. This work is financially supported by the Delft University of Technology and is part of a Materials Innovation Institute (M2i) research program with Project Number MC6.06283.

References

[1] L. Bortolotto, R. Dittmeyer, Sep. Purif. Technol. 73 (1) (2010) 51–58.
[2] R. Dittmeyer, V. Hollein, K. Daub, J. Mol. Catal. A – Chem. 173 (1–2) (2001) 135–184.
[3] K. Sato et al., Catal. Today 156 (3–4) (2010) 276–281.
[4] M. Sheintuch, R.M. Dessau, Chem. Eng. Sci. 51 (4) (1996) 535–547.
[5] F. Gallucci et al., Ind. Eng. Chem. Res. 45 (9) (2006) 2994–3000.
[6] S. Uemiya, Top. Catal. 29 (1–2) (2004) 79–84.
[7] S. Uemiya et al., Appl. Catal. 67 (2) (1991) 223–230.
[8] R.J. Westerwaal et al., Int. J. Hydrogen Energy 38 (10) (2013) 4201–4212.
[9] D.E. Nanu, A.J. Bottger, Adv. Funct. Mater. 18 (6) (2008) 898–906.
[10] H. Amandusson, L.G. Ekedahl, H. Dannetun, Appl. Surf. Sci. 153 (4) (2000) 259–267.
[11] H.Y. Gao et al., Ind. Eng. Chem. Res. 43 (22) (2004) 6920–6930.
[12] A. Li, W. Liang, R. Hughes, J. Membr. Sci. 165 (1) (2000) 135–141.
[13] Z.Y. Zhao et al., Sens. Actuators B – Chem. 129 (2) (2008) 726–733.
[14] L. Piccolo, A. Piednoir, J.C. Bertolini, Surf. Sci. 592 (1–3) (2005) 169–181.
[15] K.W. Wang, S.R. Chung, T.P. Perng, J. Alloys Compd. 417 (1–2) (2006) 60–62.
[16] F. Roa, Palladium–copper and palladium–gold alloy composite membranes for hydrogen separations, in: A.C. Bose (Ed.), Inorganic Membranes for Energy and Environmental Applications, Springer Science + Business Media, New York, USA, 2009.
[17] T. Hubert et al., Sens. Actuators B – Chem. 157 (2) (2011) 329–352.
[18] A.J. Bard, L.R. Faulkner, Electrochemical Methods Fundamentals and Applications, John Wiley & Sons, New York, 1980.
[19] A. Czerwinski, R. Marassi, J. Electroanal. Chem. 322 (1–2) (1992) 373–381.
[20] A. Czerwinski, R. Marassi, S. Zamponi, J. Electroanal. Chem. 316 (1–2) (1991) 211–221.
[21] A. Czerwinski et al., J. Electroanal. Chem. 386 (1–2) (1995) 207–211.
[22] M. Lukaszewski, A. Czerwinski, Electrochim. Acta 48 (17) (2003) 2435–2445.
[23] M. Lukaszewski, A. Czerwinski, J. Solid State Electrochem. 12 (12) (2008) 1589–1598.
[24] M. Lukaszewski, K. Hubkowska, A. Czerwinski, Phys. Chem. Chem. Phys. 12 (43) (2010) 14567–14572.
[25] M. Lukaszewski et al., J. Solid State Electrochem. 7 (2) (2003) 69–76.
[26] N.M.v. d Pers et al., A diffracted-beam monochromator for long linear detectors in X-ray diffractometers with Bragg–Brentano parafocusing geometry, Rev. Sci. Instrum. 84 (4) (2013) 045102.
[27] M. Pourbaix, Atlas of Electrochemical Equilibria in Aqueous Solutions, NACE International, 1974.
[28] M. Lukaszewski, K. Hubkowska, A. Czerwinski, J. Electroanal. Chem. 651 (2) (2011) 131–142.
[29] K. Hubkowska et al., J. Electroanal. Chem. 704 (2013) 10–18.
[30] H. Conrad, G. Ertl, E.E. Latta, Surf. Sci. 41 (2) (1974) 435–446.
[31] P. Perrot, Gold–Hydrogen–Palladium, Landolt–Bornstein, 2006, pp. 258–265.
[32] C.G. Sonwane, J. Wilcox, Y.H. Ma, J. Phys. Chem. B 110 (48) (2006) 24549–24558.
[33] C.G. Sonwane, J. Wilcox, Y.H. Ma, Achieving optimum hydrogen permeability in PdAg and PdAu alloys, J. Chem. Phys. 125 (18) (2006) 45.
[34] J.L. Rousset, J.C. Bertolini, P. Miegge, Phys. Rev. B 53 (8) (1996) 4947–4957.
[35] E.J. Mittemeijer, U. Welzel (Eds.), Modern Diffraction Methods, Wiley-VCH Verlag & Co.: Weinheim, Germany, 2013.
[36] D. Tomanek et al., Surf. Sci. 114 (1) (1982) 11–22.
[37] S. Luo, D. Wang, T.B. Flanagan, J. Phys. Chem. B 114 (18) (2010) 6117–6125.
[38] D.E. Nanu et al., Acta Mater. 58 (16) (2010) 5502–5510.
[39] F.E. Wagner et al., Interaction of hydrogen with substitutional solute metals in the β-phase of the palladium–hydrogen system, in: P. Jena, C.B. Satterthwaite (Eds.), Electronic Structure and Properties of Hydrogen in Metals, Springer, US, 1983, pp. 581–588.
[40] A. Maeland, T.B. Flanagan, J. Phys. Chem. 69 (10) (1965) 3575.
[41] M. Lukaszewski et al., Materials 6 (10) (2013) 4817–4835.